International Journal of Automotive Technology, Vol. 4, No. 1, pp. 31–40 (2003)

1229–9138/2003/011–04

DYNAMIC CHARACTERISTICS OF SCALED-DOWN W-BEAMS UNDER IMPACT

T. Y. J. HUI, H. H. RUAN and T. X. YU*

Department of Mechanical Engineering, Hong Kong University of Science and Technology, Clear Water Bay, Kowloon, Hong Kong

(Received 31 October 2002; Revised 14 February 2003)

ABSTRACT–W-beam guardrail system has been the most popular roadside safety device around the world. Through large plastic deformation and corresponding energy dissipation, a W-beam guardrail system contains and re-directs out-of-control vehicles so as to reduce the impact damage on the vehicle occupants and the vehicles themselves. In this paper, our recent experiments on 1:3.75 downscaled W-beam and the beam-post system are reported. The static and impact test results on the load characteristics, the global response and the local cross-sectional distortion are reveled. The effects of three different end-boundary conditions for the beam-only testing are examined. It is found that the load characteristics are much dependent on the combined contribution of the local cross-sectional distortion and the end-supporting conditions. The energy partitioning between the beam and the supporting posts in the beam-post-system testing were also examined. The results showed that the energy dissipation partitioning changed with the input impact energy. Finally, a simple mass-spring model is developed to assess the dynamic response of a W-beam guardrail system in response to an impact loading. The model's prediction agrees well with the experimental results.

KEY WORDS : Guardrail system, W-beam, Dynamic characteristics, Energy partitioning, Cross-sectional distortion, Mass-spring model

1. INTRODUCTION

Roadside safety devices are used to reduce the severity of the impact to the car as well as the car occupants in a crash event by dissipating a large amount of the kinetic energy of the collision. Therefore, they are of crucial importance to road users' safety. W-beam guardrail systems have been the most popular roadside safety device for the last few decades and, thus, their behavior under impact loading is worth a throughout investigation.

Full-scale testing for the performance of the W-beam guardrail system has been conducted in the United States (Bank *et al.*, 1998a) and Japan (Ando *et al.*, 1995). However, to repeat a full-scale impact testing on a guardrail system would be very tedious and expensive. As a result, attempts were made to simplify the testing procedure into a downscaled prototype (Bank *et al.*, 1998b) so that more tests could be conducted with a better controlled test input and well-recorded documentation for the dynamic response of the guardrail. This downscaled testing has been used as a screening process for the selection of new guardrail material and guardrail cross-sectional profile. Besides, as shown by Teh and Yu (1987) in their study of beams of angle-section, more details of the load-carrying capacity and local cross-sectional distortion could be revealed because of the repeatability of the experiment. The static performance of one-third downscaled W-beams was preliminarily investigated by Hui and Yu (2000).

In the experiments reported in this paper, a downscaled prototype of the W-beam guardrail system, with a scaling factor $\beta = 1/3.75$, was adopted to conduct more tests with well-controlled input so that the record on the mechanical behavior of the beam and the system became more complete. Moreover, the experiments were divided into two main categories. The first set of tests was concentrated on the static and dynamic characteristics of the downscaled W-beam itself. After revealing the beam's behavior, two downscaled supporting posts were attached to each of the W-beam samples to form a downscaled prototype of one segment of the guardrail system to better represent the real situation in a vehicle-guardrail-system impact.

The characteristic behavior of the guardrail system obtained from the downscaled testing was then used to develop a simple mass-spring model to assess the energy dissipation and the global deformation for a

**Corresponding author*. e-mail: metxyu@ust.hk

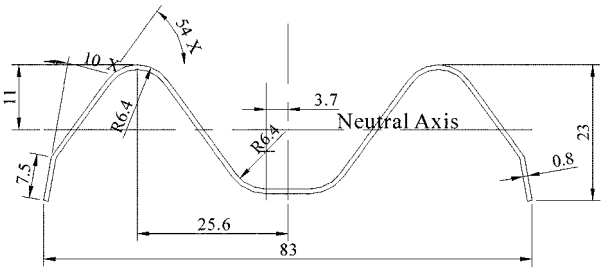

Figure 1. Cross-sectional profile of 1:3.75 downscaled W-beam.

vehicle impact on a W-beam guardrail system. The model's prediction is compared with the downscaled test results.

2. TEST METHOD AND EXPERIMENTAL SETUP

Quasi-static and dynamic tests were conducted on a geometrically downscaled prototype of the actual W-beam guardrail system to acquire the response characteristics. A scaling factor $\beta = 1/3.75$ was adopted. The cross-sectional profile of the downscaled W-beam samples and the dimensions of the downscaled supporting posts are shown in Figure 1 and Table 1, respectively. Apart from the sample size, other geometrical features, such as the supported span of the W-beam, were also downscaled by the factor β. The material of the samples was also chosen to have a compatible property of the real beams. The corresponding tensile test results for the two materials are depicted in Figure 2.

For the beam testing, beam samples of 600 mm were quasi-statically and impact three-point bended with a supporting span L of 535 mm, as shown in Figure 3. The beam samples were loaded at the mid-span by a rigid wedge head perpendicular to the beam axis. Three supporting conditions were adopted to examine their effects on the load-carrying capacity: namely (1) simply roller-supported (RS); (2) axially-constrained roller-supported (AR); and (3) simply box-supported (BS). On the roller support, the cross-section of the beam was transversely constrained; while on the box support, the corresponding edges of the cross-section were allowed to rotate freely.

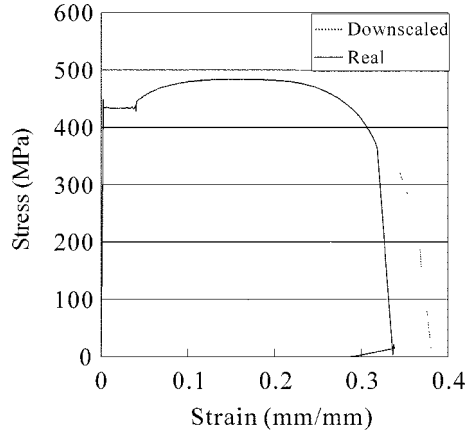

Figure 2. Typical material tensile test results for real and downscaled beams with a loading rate of 1mm/min.

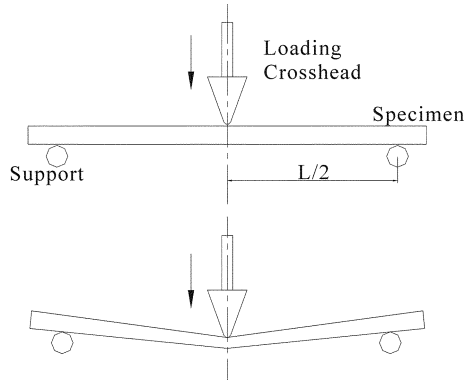

Figure 3. Schematic illustration of experimental configuration.

In the static tests, a crosshead speed of 5 mm/min was used and the load was removed at every 10 mm-interval until a final transverse displacement of 120 mm was reached. In the impact tests, the downscaled beam samples were impacted by a wedge-headed drop weight assembly of 12.92 kg at three prescribed impact velocities.

For the system testing, similar configurations as those in the beam testing was used, except that the beams were mounted on two supporting posts, one at each end, for impact loading. The system test configuration was

Table 1. Comparisons of dimensions of conventional guardrail system and the experimental setup.

	W-beam		Circular hollow post		Rectangular hollow post		
	Width	Thickness	Diameter	Thickness	Width	Height	Thickness
Original system	310-317 mm	3 mm	115 mm	4 mm	50 mm	100 mm	5 mm
Scale-down system	81-84 mm	0.8 mm	30 mm	0.8 mm	13 mm	25 mm	1 mm
Ratio	3.77-3.83	3.75	3.83	5.00	3.85	4.00	5.00

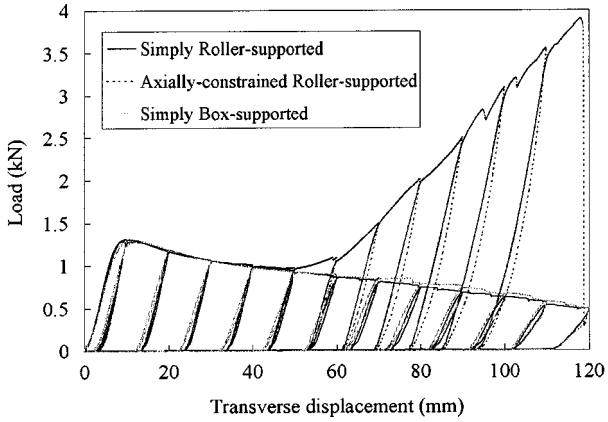

Figure 4. Load versus transverse displacement curves for quasi-static three-point bending of downscaled W-beams with different supporting end conditions.

designed according to the conventionally used guardrail system. The two supporting posts were clamped at the roots and the distance between the bolt connection to the scaled-down W-beam and the clamped end was set to be 160 mm. Two post types were tested, namely the circular hollow tubes and the rectangular hollow tubes, to compare their performances.

3. TEST RESULTS AND DISCUSSION

3.1. Quasi-static Tests on Downscaled W-beams

The load-transverse-displacement curves of downscaled W-beams are depicted in Figure 4. In general, the load-carrying capacities of the beams with different end conditions were similar: the load rose rapidly to a peak then decreased gradually. However, the notable difference was that for axially-constrained roller-supported W-beam, the load-carrying capacity rose again to a very high value at larger transverse displacement. As a sign of the structure's limit instability, the initial peak load indicates that material's hardening effect was gradually overwhelmed by the structural softening effect resulted from the serious distortion of the local cross-section at the mid-span, which reduced its second moment and thus the fully plastic bending moment. This structural softening effect also led to further localization of the deformation around the mid-span of the beam. The very localized plastic deformation was verified by the strain measurements at the mid-span and the quarter-span, as shown in Figure 5. For the axially-constrained roller-supported beams, the difference in the load-carrying capacity at larger transverse displacement was attributed to the tensile force resulted from the axial constraints, which strengthened the structure, competed with the structural softening effect and made the load rose again.

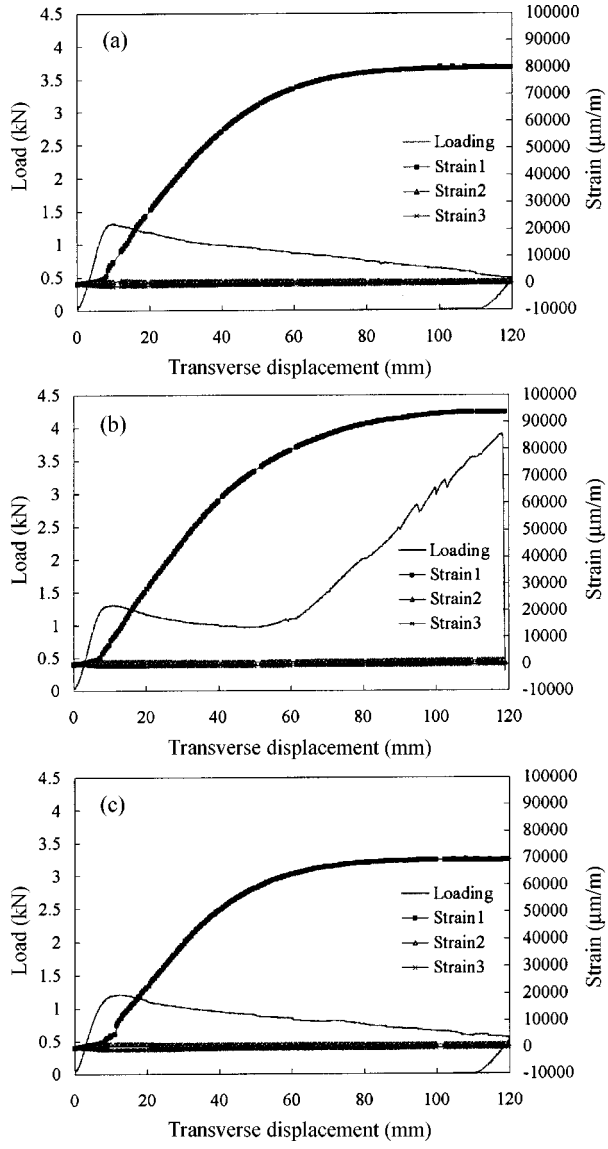

Figure 5. Strain measurements for downscaled W-beams under quasi-static three-point bending with different end supporting conditions: (a) simply roller-supported (RS), (b) axially-constrained roller-supported (AR) and (c) simply box-supported (BS). (Note: Locations of strain measurement: Strain1–mid-span, bottom; Strain2–quarter-span, bottom; and Strain3–quarter-span, top.)

The corresponding local cross-sectional distortions of the downscaled W-beams at different transverse displacements are shown in Figure 6. Despite the similarity in the load-carrying capacities, the local cross-sectional distortions accompanied the flexural deformation of the beam samples under roller and box supports were different. As observed from the measurements, under these two supporting conditions, the local cross-sectional distortions

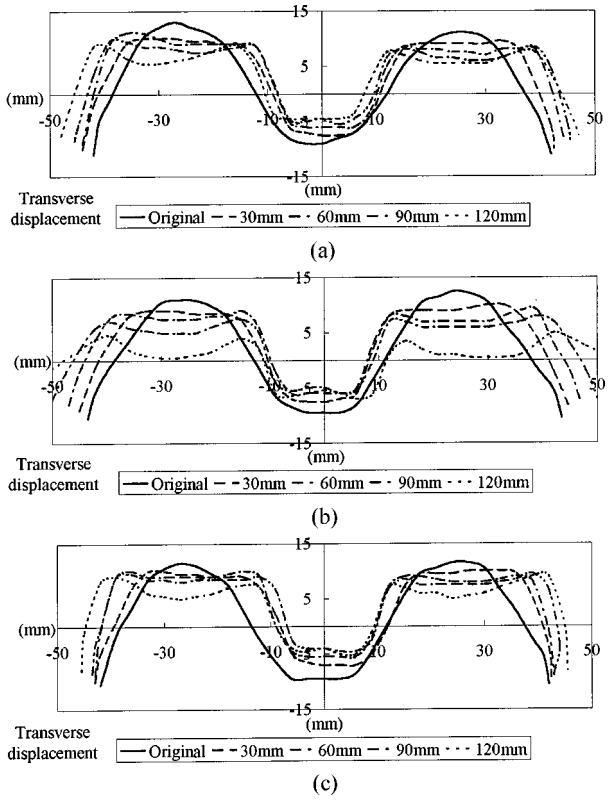

Figure 6. Local cross-sectional distortion at different transverse displacements for downscaled W-beams under quasi-static three-point bending with different end supporting conditions: (a) simply roller-supported (RS), (b) axially-constrained roller-supported (AR), and (c) simply box-supported (BS).

began with the flattening of the top portions, followed by a further collapse of the whole cross-section with bulges formed at the top. Starting from a transverse displacement of 40 mm, there was less increase in the width of the local cross-section for the simply box-supported beams. This was mainly because, for the box-supported samples, the two ends of the cross-sections were free to rotate. When larger transverse displacement was reached, the two sidewalls of the cross-sections were pushed downward. This small downward displacement of the sidewalls was not localized but occurred throughout the whole W-beam. Again, for the axially-constrained roller-supported beams, the local cross-sectional distortion was similar to its simply supported counterpart. However, heading to larger transverse displacement, the distortion deviated. Comparing the shapes of the beams at the same transverse displacement, the distortion of the local cross-section or the increase in the width for the two types of roller-supported beams was more significant than the beam samples under box-support conditions.

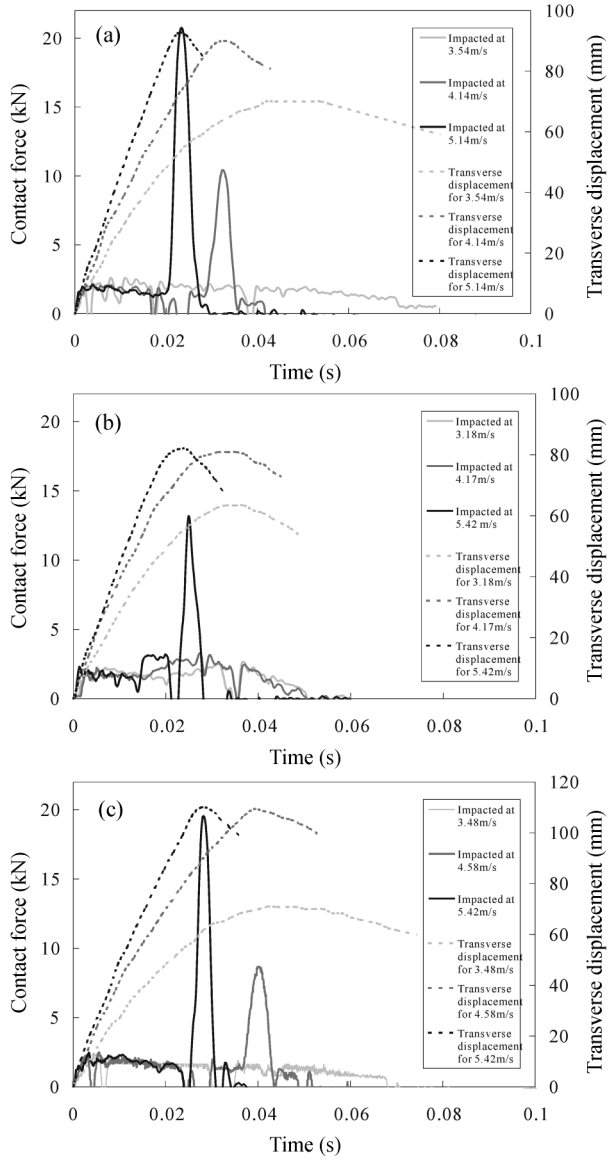

Figure 7. Contact force and transverse displacement for downscaled W-beams under impact loading with different end supporting conditions: (a) simply roller-supported (RS), (b) axially-constrained roller-supported (AR), and (c) simply box-supported (BS).

From the viewpoint of solid mechanics, during the bending process of a beam of thin-walled cross-section, some cross-sectional distortions must occur and accompany the flexural deformation to make the total deformation energy of the beam minimum. The similar phenomenon has been previously observed and analyzed for four-point bending of beams of angle-section (Teh and Yu, 1987).

3.2. Impact Tests on Downscaled W-beams

Figure 7 demonstrates the contact-load characteristics

during the first impact of the downscaled W-beams with different end supporting conditions under three different impact velocities. There were two peaks in the contact load history: an initial peak and a highest peak. The initial peak loads for all impact velocities and end supporting conditions were similar, approximately 1.5 times their static counterparts. The increase is attributed to the strain rate effect of the material and the inertia effect of the beam. Yet, another observation from the contact load characteristics is that there was a sudden increase in the load when the drop weight reached its maximum transverse displacement and just started to rebound. This phenomenon was more notable when the initial impact velocity increased, resulting in a corresponding higher peak load. For lower velocity impacts, this sharp increase might be absent. Normally, for all simply supported beams, an impact velocity larger than 4 m/s would induce such a sharp contact load. Yet, for the beams with extra axial constraints, this phenomenon occurred only when the impact velocity was beyond 5 m/s and the peak value was considerably smaller. As observed from the high-speed videos taken, one possible explanation is that when the beam was hit by the drop head with a lower velocity, the deceleration and the increase in the transverse displacement would be more gradual, and thus the change in velocity would be slow and the load characteristics would be more like a plateau. However, when the beam was hit with a higher velocity, the deceleration and the increase in the transverse displacement would be more abrupt towards the end of the impact event; therefore, there would be an abrupt increase in contact-load induced. As for beams with extra axial constraints, the constraints helped in the reduction of the velocity of the drop head in the early stage, making the final change in velocity near the end of the impact event less sudden.

The local cross-sectional distortion mechanism of the beams under impact was found to be very similar to those in the static three-point bending. For all supporting conditions, there was a flattening of the top portions of the local cross-section under the drop head. With the increase in impact velocity, there was further collapse of the local cross-section. Yet, nearly all the deformation was localized in the 'plastic zone' underneath the line of drop head, forming bulges and elongating the material in the zone as in the static tests. One difference in the cross-sectional distortions observed between the quasi-statically and impact tested down-scaled W-beams is that for the impact-tested samples, with a final transverse displacement similar to its quasi-static counterpart, the cross-sectional distortion was less severe, as shown in Figure 8. The distortion zone in the quasi-static case was longer along the axial direction and the distorted cross-section was wider.

Another parameter was introduced here to evaluate the change in the local cross-section. The second moment of the cross-section at the mid-span before (I) and after (I') the impact event were calculated from the measured profiles. As an index of the change in the beam's flexural stiffness, the ratio I'/I indicates the change in the second moment, as plotted in Figure 9.

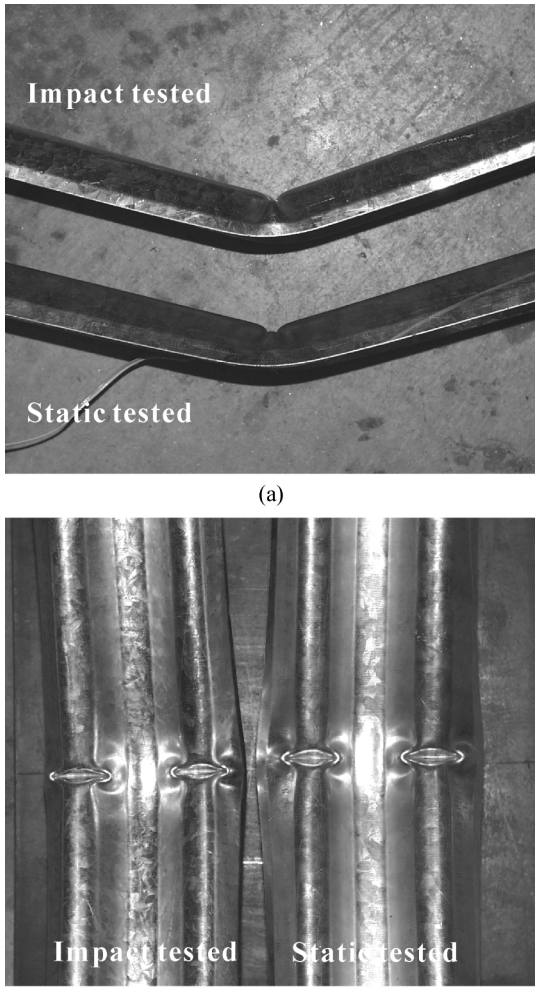

Figure 8. Comparison between the local cross-sectional distortion of static and impact tested downscaled W-beams with a similar final transverse displacement, (a) bird view; (b) side view.

3.3. Impact Tests on Downscaled W-beam Systems

Figure 10 depicts the contact-load characteristics during the first impact of the downscaled system with different supporting posts. Similar to that observed in the beam tests, there was an initial peak load followed by a very high and sharp peak towards the end of the impact event when the impact velocity was high, despite the type of supporting posts. The sudden-risen highest load occurred

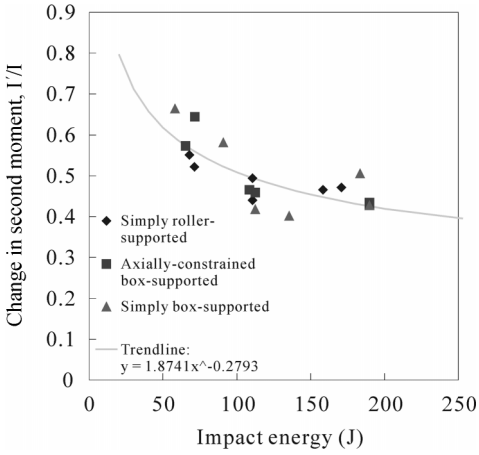

Figure 9. Change in the second moment of the local cross-section as a function of input energy for impact tests of downscaled W-beams with different end supporting conditions.

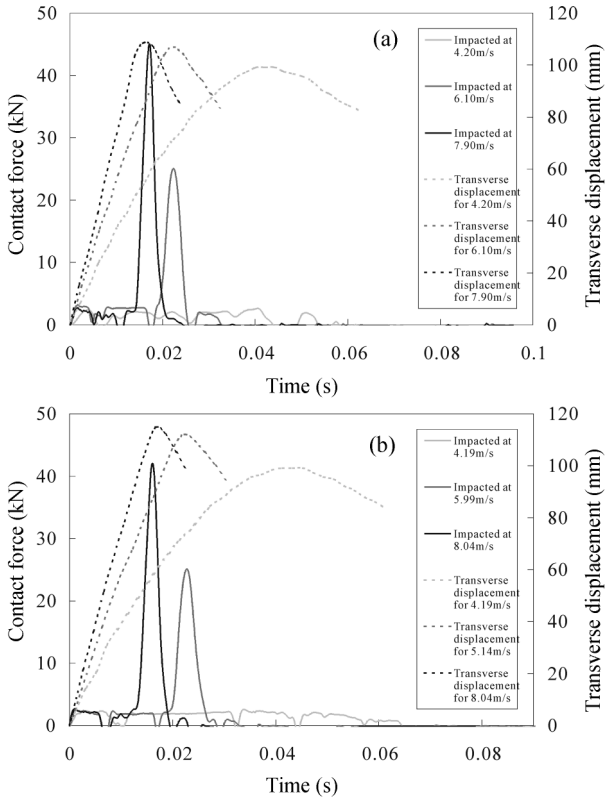

Figure 10. Contact force and transverse displacement versus time for downscaled guardrail systems with (a) rectangular hollow posts and (b) circular hollow posts.

when the transverse displacement reached the maximum. The initial peak loads were of a similar value as those in

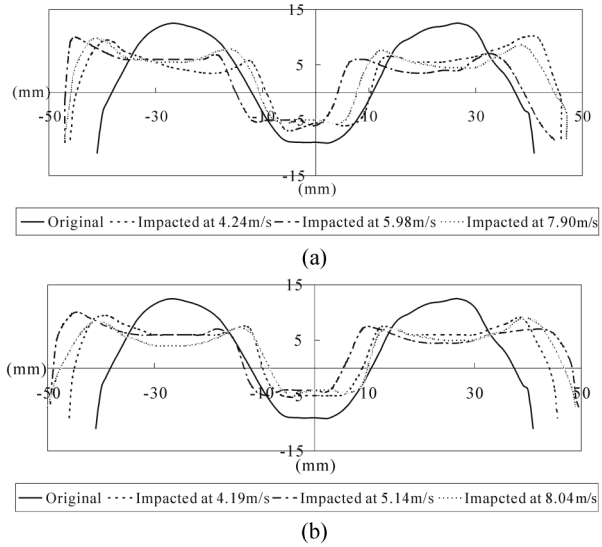

Figure 11. Local cross-sectional distortion for different impact velocities with (a) rectangular hollow posts and (b) circular hollow posts. (Note: right end: supported by the post; left end: hanging freely).

the beam impact tests. This is reasonable because, as observed from the high-speed videos, during the early stage of the response only the beam deformed, which was then followed by the bending deformation of the supporting posts when the drop head reached a larger displacement. The reason for the sudden peak near the end of the impact event is similar to that in the beam-only tests.

There was no considerable difference in the distorted shape of local cross-section for beams with different supporting posts. There was still flattening and bulge formation at the top portions of the local cross-section found in the system-tested beams. Nonetheless, compared with the cross-sectional distortions of the beams in the beam-only tests, the distorted shapes in the system tests were very much asymmetric (Figure 11), unlike those resulted from the quasi-static or impact tests of the beam alone. It is because the two sides in the beam's width direction were in a different supporting condition during the system test. For the side near the clamped end, the beam's end cross-section was supported by the post, like with a roller support; while the other side was hang freely, like with a box support. When the beam was hit by a drop head and the cross-section started to distort, the rotational motion of the sidewall of the cross-section near the clamped end was constrained by the supported post; and the freely hang sidewall was free to rotate. Therefore, it was observed from the records that a half of the distorted local cross-section was more flattened; while the other half displayed more inward motion of the

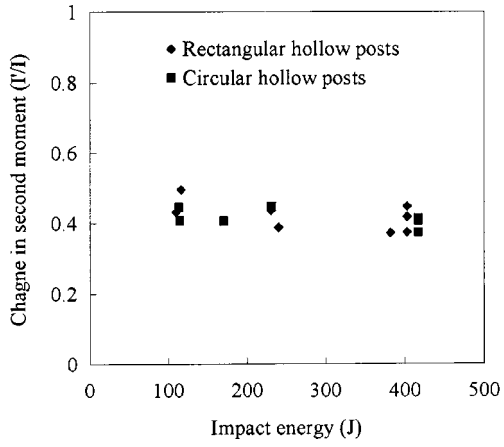

Figure 12. Change in the second moment of the local cross-section as a function of impact energy for impact tests of downscaled guardrail systems with different supporting posts.

sidewall. Again, the change in second moment, ratio *I'/I*, of the local cross-sections is plotted in Figure 12. Unlike the results in the beam-only tests, the values of this ratio of second moment remained almost the same for different input impact energies. As shown below, when the input impact energy was higher, the supporting posts dissipated more energy, so that the flexural deformation as well as the local cross-sectional distortion in the guardrail beam-post system would become less sensitive to the input energy.

The final deformation of the W-beam in a system test was measured after the test when the beam was dismounted. The energy dissipation partitioning between the down-scaled W-beam and the supporting posts can then be evaluated from the final deformation of the W-beam,

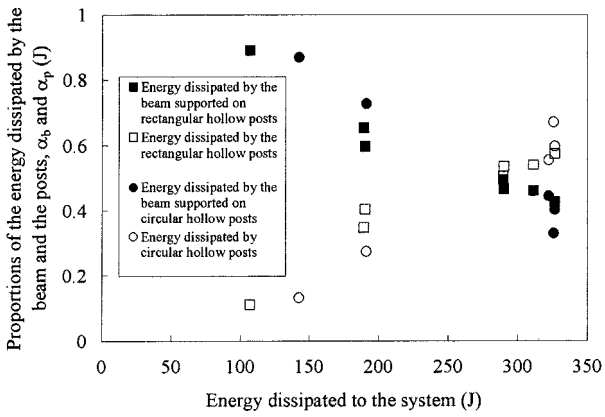

Figure 13. Proportions of the energies dissipated by beam and posts under impact loading, varies with the total energy dissipation in the beam-post system.

because the energy dissipated by the beam alone till this final deformation can be estimated based on the results of the beam-only tests. The correlation for the simply supported beams is used for the estimate, and the energy dissipation ratio α_b and α_p are plotted against the total energy dissipated by the system. Here α_b and α_p are defined as

α_b=(Energy dissipated by the beam)/(Total energy dissipated by the system)

α_p=(Energy dissipated by the posts)/(Total energy dissipated by the system)

respectively. As observed from Figure 13, when the impact energy was low, the W-beam dissipated most of the input energy; when the impact energy was high, the supporting posts shared more portion of the input energy, and eventually shared a portion larger than that of the W-beam.

4. DEVELOPMENT OF A MASS-SPRING MODEL

In the evaluation of a guardrail system, there are many possible combinations of rail and post materials and shape profiles. Therefore, a theoretical model should be developed and it should be capable of predicting the dynamic behavior of the guardrail-post system, with the essential physics of the impact event on the system being preserved.

In general, the dynamic response of a structure is mainly governed by the inertia and the dynamic resistance of the structure, such as that shown in Figure 14. The first factor is described by the mass or equivalent mass of the structure, whilst the second factor is represented by the load-carrying capacity associated with the deformation mechanism of the structure. As a result, the dynamic behavior of a simple structure can be modeled by a single degree-of-freedom mass-spring model, which significantly simplifies the problem without losing the fundamental physics of the impact event. Symonds and Frye (1988) studied a single degree-of-freedom mass-spring system to represent a rigid-plastic response of structures in an impact event. Wu and Yu (2001) also proposed two lumped-mass-spring models, namely the stick and non-stick models, to predict the dynamic behavior of a

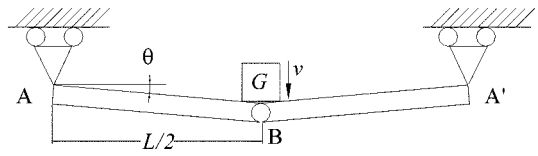

Figure 14. Single-hinge mechanism for a simply supported beam with no axial constraints subjected to an impulsive load at the mid-span.

structure under a rigid-projectile's impact; and examined the applicability of the simple mass-spring model on the dynamic deformation of elastic-plastic structures.

For the single-hinge deformation mechanism in our current problem (Figure 14), because the striking mass is much larger than that of the guardrail beam, the Modal Approximation Technique (MAT) proposed by Martin and Symonds (1966) can be adopted and the response of the downscaled guardrail beam is then transformed into a single degree-of-freedom problem. Based on the same reason, the stick assumption (Wu and Yu, 2001) is adopted. By re-examining the formulation, the corresponding governing equation is written as:

$$\frac{1}{3}\rho\left(\frac{L}{2}\right)^3\ddot{\theta}+\frac{G}{2}\left(\frac{L}{2}\right)^2\ddot{\theta}=M_B \quad \text{for a simply-supported beam} \tag{1}$$

where ρ is the density per unit length of the beam, L is the span of the beam between the supports, θ is the angle of rotation at the supports, G is the mass of the drop weight assembly, and M_B is the bending moment at section B, as shown in Figure 15(a). Taking $m_b=(1/3)\rho L$ and $F=4M_B/L$ as the equivalent mass and the characteristic load of the beam, respectively, the governing equation is recast as

$$(G+m_b)\dot{v}=F \quad \text{for a simply-supported beam} \tag{2}$$

where $\dot{v}=\frac{L}{2}\ddot{\theta}$.

Similarly, we find

$$\frac{1}{3}\rho\left(\frac{L}{2}\right)^3\ddot{\theta}+\frac{G}{2}\left(\frac{L}{2}\right)^2\ddot{\theta}=M_B+N\left(\theta\cdot\frac{L}{2}\right)$$

for an axially-constrained beam (3)

where N is the induced axial force by the extra axial constraints at the supports, as shown in Figure 15(b). And by taking the equivalent mass $m_b=(1/3)\rho L$ and the characteristic load $F'=4M_B/L+2N\theta$, the governing equation is recast as

$$(G+m_b)\dot{v}=F' \quad \text{for an axially-constrained beam} \tag{4}$$

The mass-spring models associated with Equations (2) and (4) are depicted in Figure 16(a).

For the modeling of a guardrail-post system, a two degree-of-freedom mass-spring system is proposed, as shown in Figure 16(b). This model is reasonable since it was observed that the deformation of the posts was concentrated at the clamped end where a single plastic hinge formed. The equivalent mass and the characteristic load of the add-on spring-mass system representing the posts' dynamic behavior can be taken as $G_p=2G_p'=(2/3)\rho_p L_p$ and $F_p=2F_p'=2(P(L_p'/L_p-M_C/L_p))$, respectively. And based on the conservation of momentum, the initial condition of the system at $t=0$ are

$$\delta_b=\delta_p=0 \tag{5}$$

$$\dot{\delta}_b=v_o \tag{6}$$

where δ_b and δ_p denote the displacement of the guardrail beam and the supporting posts in the y-direction, respectively, and v_o is the impact velocity of the striking mass G.

The characteristic load of the downscaled W-beam and the supporting posts can then be obtained from their static test results. However, many additional effects contribute to the dynamic behavior of the structural system, making the latter very different from its quasi-static counterpart. Consequently, a "**dynamic enhancement factor**" has been introduced in our modeling to modify the static load characteristics of the structures. This factor accounts for the combination of the strain-rate effect of the material, the lateral inertia effect of the structure and the dynamic effect on the flexural stiffness of the beam related to the

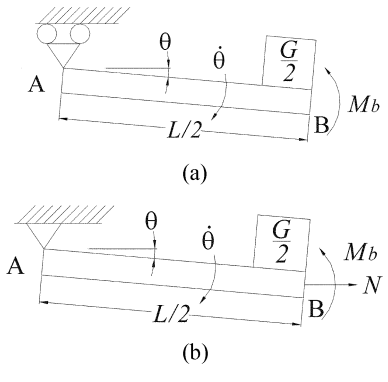

Figure 15. Deformation mechanism of a half of (a) a simply-supported and (b) an axially-constrained beam subjected to a striking mass G at the mid-span.

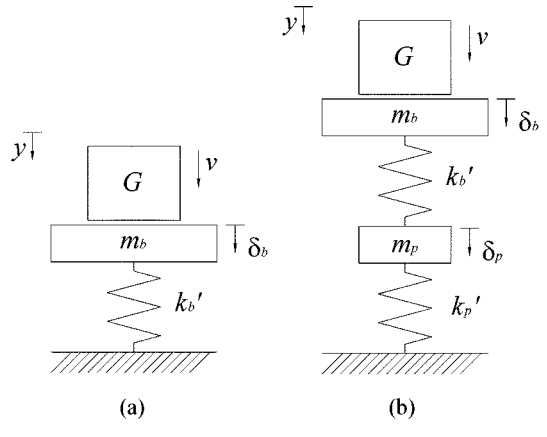

Figure 16. Mass-spring models of (a) a W-beam and (b) a W-beam guardrail system under impact by a striking mass G.

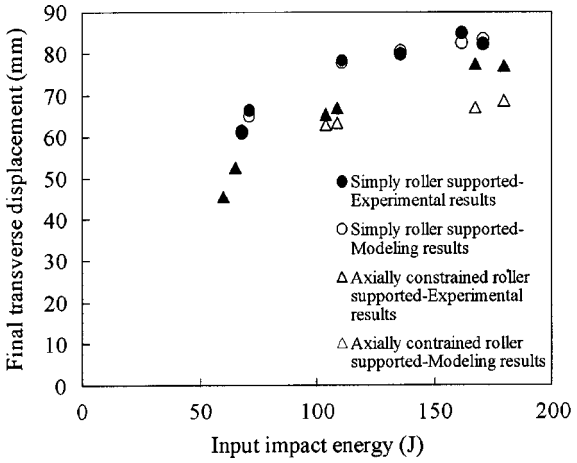

Figure 17. Experimental results and numerical predictions for downscaled W-beam tests with different end supporting conditions.

distortion of the local cross-section under impact.

The "dynamic enhancement factor" is defined as:

$$\eta = \frac{E^D\big|_{\delta_b}}{E^S\big|_{\delta_b}} \tag{7}$$

where $E^D\big|_{\delta_b}$ and $E^S\big|_{\delta_b}$ denote the input energies required to achieve transverse displacement δ_b in impact test and in the static test, respectively.

Utilizing the above formulations, Figure 17 depicts the numerical predictions together with the corresponding experimental results for the beam-only tests; while Table 2 summarizes the comparison between the experimental results and the numerical predictions for the downscaled guardrail system with circular hollow posts, when different end boundary conditions are applied. Since the end boundary condition in the system testing was a situation between simply-support and axially-constrained-support due to the possible two-directional bending of the downscaled supporting posts, the numerical predictions based on the two assumptions are shown for comparison.

5. CONCLUSION

As observed from the downscaled experiments, the performance of a W-beam under different end supporting conditions is mainly affected by three factors: (1) the material's strain hardening, (2) the structural softening due to the local cross-sectional distortion, and (3) the tensile forces caused by the axial constraints.

For the downscaled guardrail-post system tests, the energy partitioning between the W-beam and the supporting posts is estimated based on the experimental measurements. It is found that the proportions of the energies dissipated by the beam and posts under impact loading varies with the total input energy in the system: more portion of the energy is dissipated by the beam when the input impact energy is low, and more portion of the energy will be absorbed by the posts when the input impact energy is higher.

Finally, a simple mass-spring model is proposed to predict the dynamic performance of the guardrail beam or the guardrail-post system subjected to impact loading, and the model's prediction has shown a good agreement with the experimental results.

ACKNOWLEDGEMENTS–The authors would like to acknowledge the support form the Hong Kong Research Grant Council (RGC) under grant HKUST6035/99E, and that from the Guangdong Province Science foundation. The assistance from the South China University of Technology (SCUT) in the manufacturing of downscaled beam is gratefully acknowledged.

REFERENCES

Ando, K., Fukuya, T., Kaji, S. and Seo, T. (1995). Development of guardrails for high speed collisions. *Transportation Research Record*, **1500**, 52–58.

Bank, L. C., Gentry, T. R. and Yin, J. (1998a). Pendulum impact tests on steel W-beam guardrails. *J. of Trans.*

Table 2. Experimental results and numerical predictions for scaled-down guardrail system with circular hollow supporting posts.

Impact velocity, m/s	Experimental final transverse displacement, mm	Predicted final displacement, with simply supported assumption, mm	Predicted final displacement, with axially constrained assumption, mm
4.19	81.15	75.84	62.96
4.21	86.07	77.16	63.11
5.14	89.34	83.30	64.97
5.99	91.81	89.26	66.48

Eng July/August, 319–325.

Bank, L. C., Hargarve, M., Svenson, A. and Teibei, A. (1998b). Impact performance of pultruded beams for highway safety applications. *Composite Structures* **42**, 231–237.

Hui, S. K. and Yu, T. X. (2000). Large plastic deformation of W-beams used as guardrails on highways, in *Advances in Engineering Plasticity, Part 2* (ed. T.X. Yu, Q. P. Sun and J. K. Kim), *Key Engineering Materials*, **177-180,** 751–756.

Martin, J. B. and Symonds, P. S. (1966). Mode approximations for impulsively-loaded rigid-plastic structures. *ASCE J. Eng. Mech. Div. Proc.* **92**(EM5), 43–66.

Symonds, P. S. and Frye, C. W. G. (1988). On the relation between rigidñplastic and elastic−plastic predictions of response to pulse loading. *Int. J. Impact. Eng.* **7,** 139–49.

Teh, L. S. and Yu, T. X. (1987). Large plastic deformation of beams of angle-section under symmetric bending. *Int. J. of Mech. Sci.* **39**(7), 829–839.

Wu, K. Q. and Yu, T. X. (2001). Simple dynamic models of elastic−plastic structures under impact. *Int. J. Impact Eng.* **25,** 735–754.